Molecular simulation of activity coefficients and the phase diagram of CH_3OH-CO_2 binary system

Jianbo Li and Lichang Wang*
Department of Chemistry and Biochemistry, Southern Illinois University, Carbondale, IL 62901, USA

Abstract

The interaction energies of five pairs of interactions: CH_3OH-CH_3OH, CH_3OH-CO_2, CO_2-CO_2, CH_3OH-CH_3CH_2OH, and CH_3CH_2OH-CH_3CH_2OH were obtained using MP2, B3LYP, and B3LYP-D3 methods. Activity coefficients of CH_3CH_2OH-CH_3OH and CH_3OH-CO_2 systems were calculated using the UNIQUAC equation and the phase diagrams of these binary systems were constructed based on the Raoult's law. The B3LYP-D3 methanol/ethanol isothermal phase diagram at 298K is in good agreement with the experimental data and the agreement is slightly better than the MP2 result and much better than the B3LYP result. Thus, the B3LYP-D3 method is promising to obtaining activity coefficients and illustrates the promise of molecular simulation of phase diagram of binary systems. A carbon dioxide/ethanol isothermal phase diagram at 230K was constructed. The current results showed that CO_2 and CH_3OH are hardly mixed under the simulation conditions.

*Corresponding author: lwang@chem.siu.edu

1. **Introduction**

For efficient and sustainable industrial processes, rational design of separation operations is essential. This requires knowledge of the activity coefficients of fluid mixtures and phase diagrams[1-4]. Therefore, although studies of catalysis[5-13], reactions[6, 14], various properties of molecules[15-20] and aggregates[21, 22] and design of new materials[23-28] for specific applications[29, 30] have garnered a lot of attention, considerable efforts have been devoted to the studies of binary systems[31, 32]. Investigations using various theories[33] and models[34] were carried out to obtain binary interaction parameter[35] and phase behaviors[36-38]. A particularly useful equation, UNIQUAC becomes a useful tool for process-design engineers to calculate fluid-phase equilibria as required in the design of distillation, extraction, and similar operations[39]. The UNIQUAC equation, using only two adjustable parameters per binary in addition to the pure-component parameters reflecting the sizes and outer surface areas of the molecules, is applied widely to calculate activity coefficients.

The UNIQUAC equations based on the representation of liquid-liquid interaction contain two parts: combinatorial and residual. The combinatorial part is a function of mole fraction, and molecular area and segment fractions. These structural parameters are based on the types and numbers of each component, and from the Van der Waals volume and surface areas of each component. The residual part of the activity coefficient is computed from mole fractions, molecular areas, and the energy of interactions between molecules. In this part, there are two parameters τ_{ij} and τ_{ji} representing the energy of interactions which are not able to be measured but must be evaluated empirically from vapor-liquid or liquid-liquid

equilibrium data[40]. Based on experimental data, Kato, et al[41] proposed that the values of the interaction energies can be correlated with a fourth- order function of $(q_j-q_i)/q_j$, where q_i and q_j denote the molecular surface area of the solute i and j, which represents binary alkane/alkane systems.

These interaction parameters could be obtained by fitting to experimental Vapor Liquid Equilibrium data, but it is not easy to obtain these parameters through experiments in the UNIQUAC equation. It is significant to find an alternative way to determine these parameters because considerable difficulty or even unfeasibility for some systems. Molecular simulation provides a promising approach to calculate the UNIQUAC parameters. Jonsdottir[42] and his coworkers found a new way to obtain these parameters, based on Molecular Mechanics (MM) with the consistent force field (CFF). In CFF model, two main types of interaction between atoms are considered: bonded interactions (chemical bonds) and non-bonded interactions (vander Waals and electrostatic), and parameters are optimized from experimental structural and spectroscopic data for pure components without any experimental data for mixtures. Interaction parameters for the UNIQUAC method have successfully been determined for n-butane/n-pentane, n-hexane/c-hexane, n-petane/n-hexane, n-pentane/acetone, acetone/cyclohexane, cyclohexane/cyclohexanone. Rasjuussen, et al[43] studied phase equilibria of carbohydrades in polar solvent with molecular mechanics method, the calculations applied in glucose/water and sucrose/water are in agreement with experiments.

Theoretical Interaction Energy Calculation (TIEC) was proposed by Cooke, et al[44] to model and measure solid-liquid and vapor-liquid equilibria of polyols and carbohydrates in aqueous solution. In this method, interaction parameters are determined between the solvent

and a model compound of similar size as the solvent molecule that contains one or two repeat units of the polymer molecule. The solubilities of monosaccharides xylose and galactose, and the disaccharides maltose monohydrate, cellobiose and trehalose dehydrate in water were measured at various temperatures in good agreement with experiment. Kjeld Rasmussen, et al[45] used this method to calculate solvent activities for the diethylketone/polypropylene system, giving results in good agreement with experimental values.

A search algorithm denoted as the Boltzmann Jump Procedure (BJP), which Klein, et al[46] and coworkers employed to determine UNIQUAC interaction parameters for alkane/amine system, was a more efficient method for sampling conformational space than the existing method before. The advantages of the BJP algorithm are that it uses a stochastic selection criterion, as in Monte Carlo simulations, in which up-hill jumps in energy are allowed, and it is thus possible to jump over energy barriers or saddle points. The temperature effect is included by calculating the Gibbs free energy at certain temperature for each pair of different locally stable conformers and using Boltzmann statistics to determine their relative probabilities. They also applied this method to carry out simulation for 1,2-ethanediol, 1,2-propanediol and glycerol, surrounded by water molecules[47]. This simulation was efficient and gave results in good agreement with the experimental data.

Due to the importance of CO_2 capture and utilization, many models for CO_2 adsorption[48-51] and capture[52-58] were proposed. Investigations were made on super critical CO_2[59-62] and of CO_2 interacting with various organic molecules[63-86]. Studies were carried out for the CO_2-CH_3CH_2OH binary system using MD simulation[87, 88] or artificial neural network approach[89-92]. Studies of CO_2-CH_3OH binary system[93, 94]

were also reported, as CH_3OH plays an important role in the super critical CO_2 system. The role of CH_3OH has been to increase the polarity and solvent strength while retaining the sensitivity of solubility with respect to pressure and temperature. Moreover, CH_3OH can improve the selectivity of separation by preferentially interacting with one or more components and facilitating selective fractional separation[95]. Fluid phase equilibria of CO_2-CH_3OH[96] using Peng-Robinson and Soave-Redlich-Kwong mixing rules.

In this work, we utilize electronic structure theory calculations to study the interaction of two binary systems, CO_2-CH_3OH and CH_3OH-CH_3CH_2OH. The objectives of the work are to determine the accuracy of MP2, B3LYP, and B3LYP-D3 in calculating the interaction energy by comparing calculated phase diagrams of the CH_3OH-CH_3CH_2OH binary system and the experimental results, and to calculate the activity coefficients and phase diagram of CO_2-CH_3OH binary system to explore whether it is feasible to study the performance of co-solvent in supercritical system using molecular simulation.

2. **Method**

Activity coefficients and constructions of phase diagrams of binary systems rely heavily on the accuracy of the results of interaction energy, which is often the character of dispersion interaction. Dispersion interactions are generally defined as the interaction between instantaneous dipole moments within the electron distributions of two atoms or molecules[97, 98]. These interactions are ubiquitous, long-range attractive forces which act between separated molecules even in the absence of charges or permanent electric moments[99]. The dispersion interactions, so-called “weak interactions” are usually underestimated in most electronic structure based computations. However, their neglect may

sum up to significant relative contributions and then lead to qualitatively wrong conclusions. This will become more important with the size of the system, because dispersion effects have a much longer range than the opposite exchange repulsion.

Density functional theory (DFT) has gained attention as an ideally cost-effective method for calculations of many chemical systems. However, conventional DFT has problems in describing weak Van der Waals interactions. The general drawback of all common density functionals such as hydrids like the popular B3LYP, is that they cannot describe long-range electron correlations that are related for the dispersion forces[100]. The problem stems from the insufficiency of both exchange and correlation functional[101]. Lacks and Gordon[102] described the issue with the exchange functionals that the behavior of the exchange energy density at the low-density-high-gradient region had the crucial unignorable influence on the interaction energies.

Lot of effort has been exerted to develop a robust dispersion correction that can be applied to common standard density functionals without any specific fitting procedure. The approach should be as simple as possible, and in particular allow the easy calculation of energy gradients for efficient geometry optimization. DFT-D method (atom pairwise sum over C_6R^{-6} potentials[103, 104]) is this kind of dispersion correction, and has been improved by lots of researchers. The DFT-D3 (recent version of DFT-D) approaches have been quite successful in describing weak dispersion interactions among carbonic systems or organic materials[105-107]. The DFT-D3 method with B97-D or BLYP functionals yields interaction energies that are very close to the best CCSD(T) reference data. The approaches have been quite successful in describing weak dispersion interactions among carbonic systems or

organic materials. One of the improvements of DFT-D3 is that the complicated, non-additive and system-dependent exchange-repulsion, electrostatic, and induction effects are very accurately described by the DFT-D3 density functionals[108]. The development of DFT-D3 has provided chemists with a valuable tool for modeling a great number of systems.

In this work, MP2, B3LYP, and B3LYP-D3 calculations were performed with the 6-311+g(d,p)) basis set using the Gaussian software to obtain the interaction energy of five pairs of interactions: CH_3OH-CH_3OH, CH_3OH-CO_2, CO_2-CO_2,CH_3OH-CH_3CH_2OH, and CH_3CH_2OH-CH_3CH_2OH. Convergence criteria are the same as these used in our previous work.[109-111] To obtain the most stable complex configuration, we used MD simulations to generate about 10 conformations for each pair and performed electronic structure calculations to determine the most stable ones.

The obtained interaction energies, u_{ij}, were used to calculate the activity coefficients from the UNIQUAC equations:

$$\ln \gamma_i = \ln \frac{\phi_i}{x_i} + (\frac{Z}{2}) q_i \ln \frac{\theta_i}{\phi_i} + l_i - \frac{\phi_i}{x_i} \sum_j x_j l_j - q_i \ln(\sum_j \theta_j \tau_{ji}) + q_i - q_i \sum \frac{\theta_j \tau_{ij}}{\sum_k \theta_k \tau_{kj}}$$

$$l_i = \frac{Z}{2}(r_i - q_i) - (r_i - 1) \qquad Z = 10$$

$$\phi_i = \frac{r_i x_i}{\sum_j r_j x_j} \qquad \theta_i = \frac{q_i x_i}{\sum_j q_j x_j} \qquad \tau_{ji} = \exp(-\frac{u_{ji} - u_{ii}}{RT})$$

where R is the gas constant, T is temperature, x_i is mole fraction of component i, γ_i is activity coefficient of i, r_i is a parameter related to the Van der Waals Volume, q_i is a parameter related to the Van der Waals surface area, and u_{ij} is the interaction energy between molecules i and j.

In order to obtain activity coefficients, in addition to the interaction energy mentioned above, two other fundamental structural parameters r_i and q_i, are required. We used the method proposed by Bondi A, et al[112] to calculate them:

$$r_i = V_i^* / (15.17 cm^3 mol^{-1})$$

$$q_i \approx A_i^* / (2.5 \times 10^9 cm^2 mol^{-1})$$

where V_i^*, A_i^* are mole Van der Waal volume and surface area. These two parameters are obtained in Materials Studio. The three parameters, vdW Scale factor, Connolly radius, solvent radius, were needed for the calculations of these parameters. The vdW scale factor is a factor specified to uniformly modify all van der Waals radii, representing a hard shell into which a probe may not pass. The Connolly radius is the radius of the Connolly probe used in calculating the atom volume field. The solvent radius is the solvent probe radius used to display solvent and accessible solvent surfaces. The van der Waals volume and surface are the volume and surface that intersect with the vdw radii of the atoms in the structure. This is equivalent to a solvent surface with a solvent probe radius of zero, a Connolly surface with a Connolly probe radius of zero and vdW scale factor of 1. The phase diagrams were generated based on the Raoult's law.

3. **Result and discussion**

3.1. The van der Waals parameters related to the volume (r_i) and area (q_i) of methanol, ethanol, and carbon dioxide

The van der Waals' contours of three molecules, methanol, ethanol, and carbon dioxide were obtained from the Materials Studio and are depicted in Figure 1. The results of r_i, q_i are provided in Table 1. These parameters together with the interaction energies will be

used to determine the activity coefficients that are used to construct the phase diagram. As shown in Table 1, the values of both parameters decrease from ethanol to methanol then to carbon dioxide.

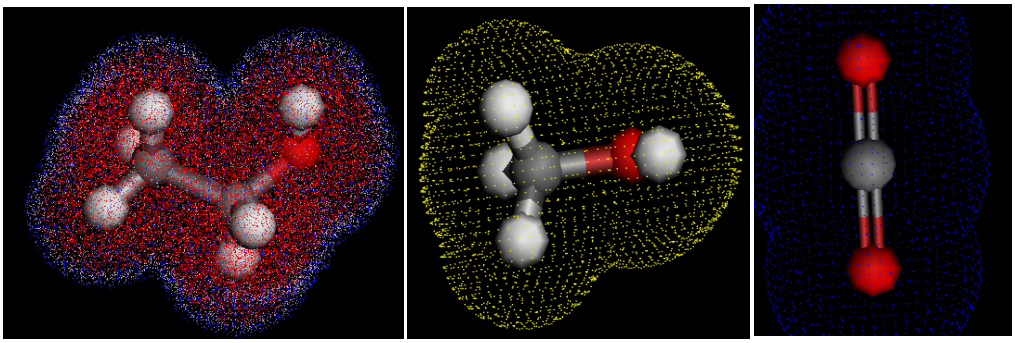

Figure 1. Description of ethanol (left), methanol (middle), and carbon dioxide (right).

Table 1. Values of *r* and *q* for ethanol, methanol, and carbon dioxide

Molecule	r_i	q_i
CH_3CH_2OH	2.1281	1.9483
CH_3OH	1.4603	1.4279
CO_2	1.3213	1.2747

3.2. methanol-ethanol system

In this research, methanol-ethanol system was studied to examine the accuracy of interaction energy using three methods and the results are provided in Figures 2-5 and Tables 2-4. For the methanol-ethanol binary system, three u_{ij} pairs are required: $u_{ethanol\text{-}ethanol}$, $u_{ethanol\text{-}ethanol}$, $u_{ethanol\text{-}ethanol}$. Take $u_{ethanol\text{-}ethanol}$ for an example, it represents the energy difference between the ethanol-ethanol stable dimer and the sum of two single ethanol molecules. Figures 2-4 show the stable structures of ethanol-ethanol, methanol-ethanol, and methanol-methanol pairs. For each pair, two different stable structures are shown after

optimizing plentiful different initial structures. It is revealed that the same character of the six stable structures is the H-bond formation. As such, the H-bond contributed dominantly to the interaction energy of the pairs. The difference between configuration a and b is on the spatial angles of alkyl groups. To illustrate each structure more clearly, we also show each structure at a different angle of view: in first one (for example a) the H-bond is parallel to the paper, while the second one (like a') is perpendicular. The optimized energies from three methods are shown in Tables 2-4. For each pair, structure b is more stable than a with MP2 and B3LYP calculations; but when adding dispersion energy, structure a is more stable than b, and one exception is that MP2 and B3LYP results for methanol-methanol are almost the same under similar structures.

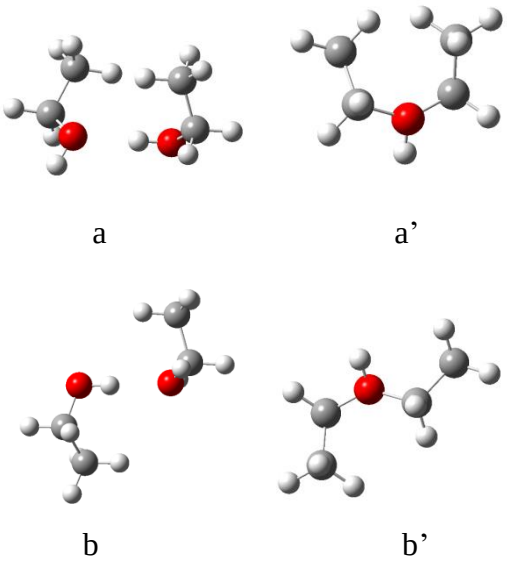

Figure 2. (a) the optimized structure of ethanol-ethanol interaction. (a').the same structure to a, but from different angle of view. (b) the second optimized structure of ethanol-ethanol interaction. (b').the same structure to b, but from different angle of view.

Table 2. Interaction energy (kJ/mol) of ethanol-ethanol pair

	Structure a	Structure b
MP2	-22.09	-22.14
B3LYP	-12.69	-13.27
B3LYP-D3	-27.77	-21.87

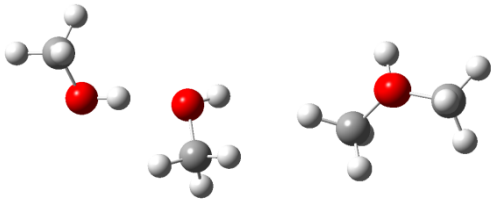

a a’

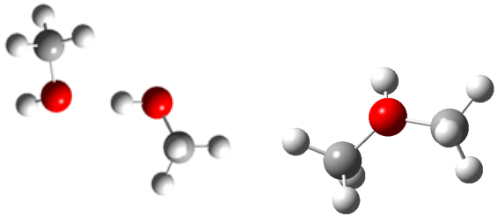

b b’

Figure 3. (a) the optimized structure of methanol-methanol interaction. (a’).the same structure to a, but from different angle of view. (b).the second optimized structure of methanol-methanol interaction. (b’) the same structure to b, but from different angle of view.

Table 3. Interaction energy (kJ/mol) of methanol-methanol pair

	Structure a	Structure b
MP2	-18.91	-18.91
B3LYP	-14.97	-14.98
B3LYP-D3	-22.72	-20.36

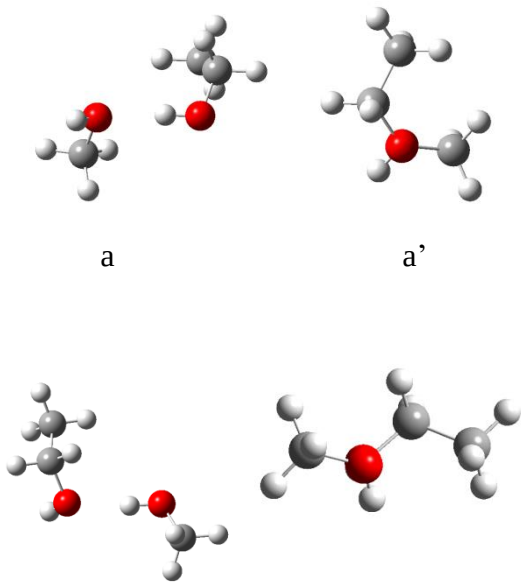

Figure 4. (a) the optimized structure of methanol-ethanol interaction. (a’).the same structure to a, but from different angle of view. (b).the second optimized structure of methanol-ethanol interaction. (b’).the same structure to b, but from different angle of view.

Table 4. Interaction energy (kJ/mol) of methanol-ethanol pair

	Structure a	Structure b
MP2	-19.99	-20.75
B3LYP	-13.27	-14.96
B3LYP-D3	-24.29	-21.87

Based on the r_i, q_i, u_{ij} results and the Raoult's law, phase diagrams of methanol-ethanol system are generated. Figure 5 shows the isotherm phase diagrams under three calculation methods comparing to experimental data (for each u_{ij}, the more optimized one is selected). From the diagrams, it is obvious that the MP2 and B3LYP-D3 calculation are in better agreement with the experimental data. The results from B3LYP-D3 is even better than that from MP2.

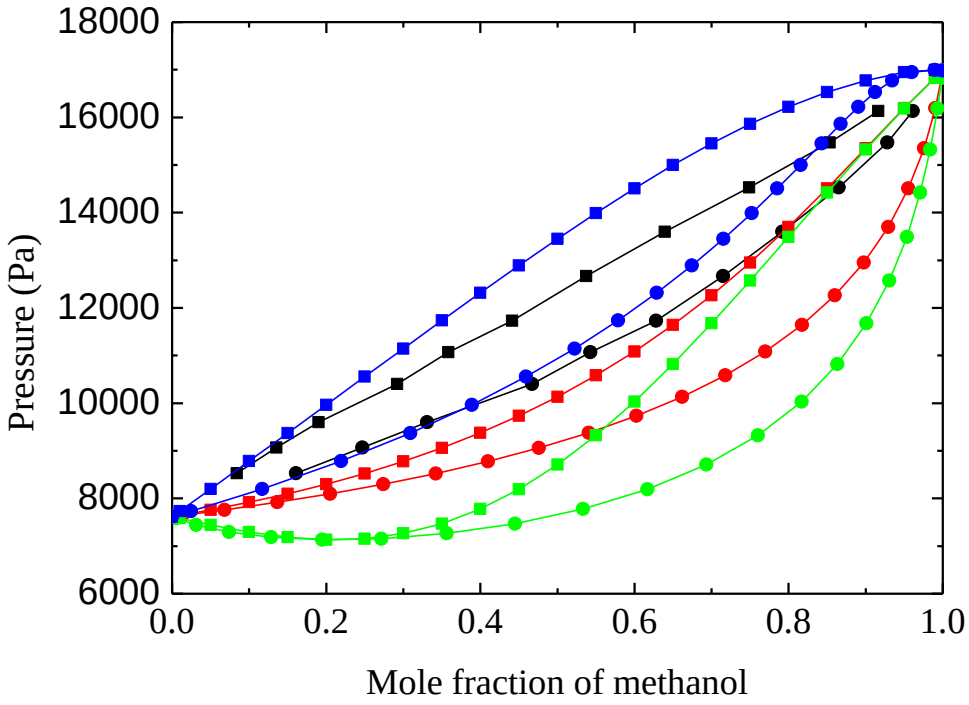

Figure 5. Isothermal phase diagram of methanol-ethanol system at 298K, where the black lines show experimental results, red, green, and blue lines denotes the results based on the MP2, B3LYP, and B3LYP-D3 calculations, respectively. Lines with squares are for liquid phase and lines with circles are for gas phase.

3.3 methanol-carbon dioxide system

The most stable structures for CO_2-CO_2 and CO_2-CH_3OH pairs are shown in Fig. 6. It is found that carbon atoms and oxygen atoms are on the same plane to form the most stable structures. Table 5 shows the interaction energy obtained by MP2, B3LYP, and B3LYP-D3, and MP2 results are more similar to that from B3LYP-D3 than that from B3LYP. We also show in Table 5 the MP2 results from different basis sets.

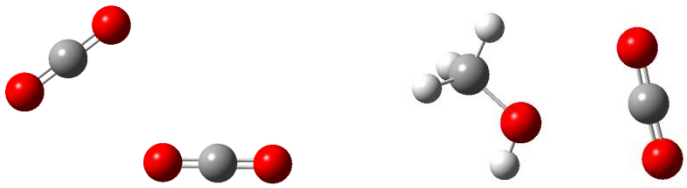

a b

Figure 6. The optimized structure of (a) carbon dioxide-carbon dioxide interaction, (b) carbon dioxide-methanol interaction.

Table 5. Interaction energy (kJ/mol) of CO_2-CO_2 and CO_2-CH_3OH pair

Interaction energy	CO_2-CO_2	CO_2-CH_3OH	Reference
MP2	-5.04	-13.8	This work
B3LYP	-1.42	-8.81	This work
B3LYP-D3	-4.95	-15.1	This work
MP2/CBS	-5.78		[113]
MP2/8s6p4d1f	-4.94		[114]
MP2/6-311+G(2df)	-5.40		[115]

Based on the parameters obtained from electronic structure calculations, we constructed the phase diagram for the methanol-carbon dioxide phase diagram. Figure 7 shows the Isothermal phase diagram of CO_2-CH_3OH system under 230K. Based on the results from methanol-ethanol binary system, the results from B3LYP-D3 prediction is the best. Indeed, the results in Fig. 7 shows that B3LYP-D3 predicted the low solubility, which is the case experimentally.[116]

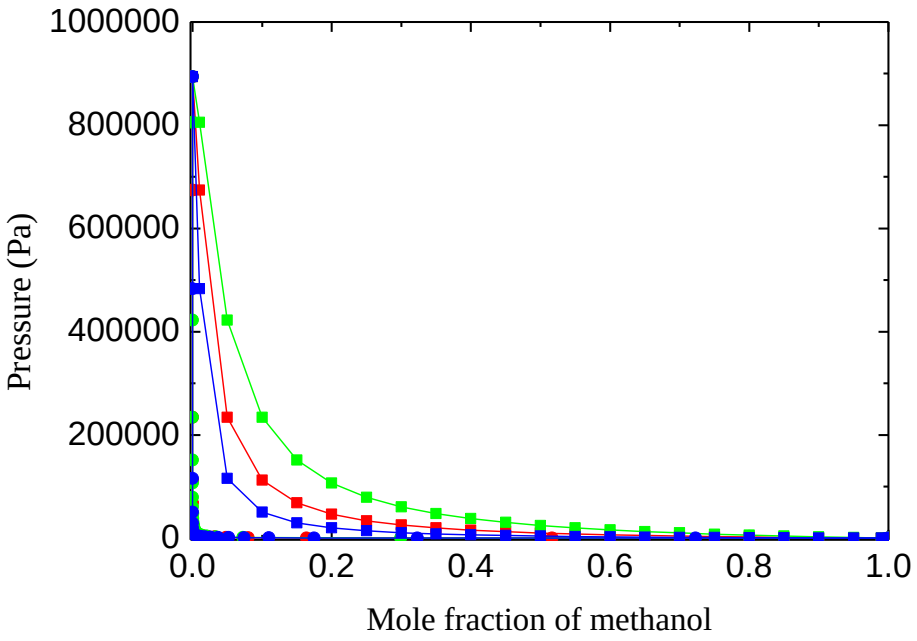

Figure 7. Isothermal phase diagram of methanol-carbon dioxide system at 230K, where the red, green, and blue lines denotes the results based on the MP2, B3LYP, and B3LYP-D3 calculations, respectively. Lines with squares are for liquid phase and lines with circles are for gas phase.

Figure 8 summarizes all u_{ij} calculation results from the five pairs obtained from the three methods. It is obvious that both the difference between B3LYP and MP2 and the difference between B3LYP-D3 and MP2 increase with the increment of interaction energy. It seems that B3LYP-D3 captures the H-bond better than MP2.

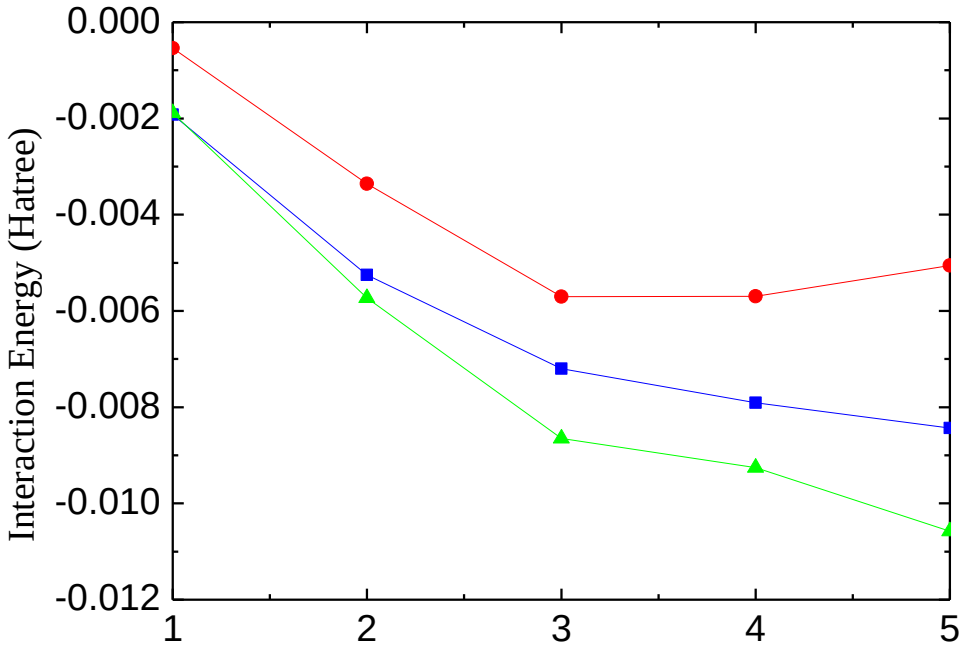

Figure 8. Comparison of the interaction energy among the MP2, B3LYP, and B3LYP-D3 calculations on five pairs of binary systems: 1:CO_2-CO_2, 2:CO_2-CH_3OH, 3:CH_3OH-CH_3OH, 4: CH_3OH-C_2H_5OH, and 5: C_2H_5OH- C_2H_5OH. Red, blue, and green lines denote the B3LYP, the MP2, and the B3LYP-D3 results, respectively.

4. **Conclusions**

Electronic structure calculations using MP2, B3LYP, and B3LYP-D3 methods were carried out to obtain interaction energies for five pairs of interactions: CH_3OH-CH_3OH, CH_3OH-CO_2, CO_2-CO_2, CH_3OH-CH_3CH_2OH, and CH_3CH_2OH-CH_3CH_2OH. Activity coefficients and phase diagrams were constructed for two binary systems: CH_3CH_2OH-CH_3OH and CH_3OH-CO_2. Comparison of CH_3CH_2OH-CH_3OH phase diagrams between the calculated and the experimental results indicate that B3LYP-D3 is the best to obtain the interaction energies. The general agreement between the B3LYP-D3 and the experimental phase diagram illustrates the promising feature of molecular simulation of

phase diagram of binary systems. Compared to the experimental data of CH_3CH_2OH-CH_3OH system, we show that the molecular simulation approach is promising to obtaining activity coefficients. The current results showed that CO_2 and CH_3OH are hardly mixed under the current simulation conditions.

Acknowledgment

J. Li acknowledges the support from the China Scholarship Council for his stay in Carbondale.

References

1. Jónsdóttir, S.Ó. and P. Rasmussen, *Phase equilibria of carbohydrates in polar solvents.* Fluid Phase Equilib., 1999. **158-160**: p. 411-418.
2. Lee, S.T., T.S. Reighard, and S.V. Olesik, *Phase diagram studies of methanol-H_2O-CO_2 and acetonitrile-H_2O-CO_2 mixtures.* Fluid Phase Equilib., 1996. **122**: p. 223-241.
3. Zhao, D., et al., *Volumetric Properties of a Binary Mixture Composed of N,N-Dimethylcyclohexylamine and Alcohols.* J. Chem. Eng. Data, 2020. **65**(4): p. 1547-1553.
4. Vishnyakov, A., et al., *Molecular models for phase equilibria of alkanes with air components and combustion products II. Alkane - Oxygen mixtures.* Fluid Phase Equilib., 2020. **520**: p. 112650.
5. Miao, B., et al., *Role of Ni in bimetallic PdNi catalysts for ethanol oxidation reaction.* J. Phys. Chem. C, 2018. **122**: p. 22448-22459.
6. Sun, K., M. Zhang, and L. Wang, *Effects of catalyst surface and hydrogen bond on ethanol dehydrogenation to ethoxy on Cu catalysts.* Chem. Phys. Lett., 2013. **585**: p. 89-94.
7. Wu, Z., et al., *Competitive C–C and C–H bond scission in the ethanol oxidation reaction on Cu(100) and the effect of an alkaline environment.* Phys. Chem. Chem. Phys., 2017. **19**: p. 15444-15453.
8. Miao, B., et al., *DFT studies on the key competing reaction steps towards complete ethanol oxidation on transition metal catalysts.* Comput. Mater. Sci., 2019. **156**: p. 175-186.
9. Wang, L., et al., *Spontaneous reduction of O_2 on PtVFe nanocatalysts.* Catal. Today, 2011. **165**: p. 150-159.
10. Xu, H., et al., *Mechanism of C–C and C–H bond cleavage in ethanol oxidation reaction on Cu_2O(111): a DFT-D and DFT+U study.* Phys. Chem. Chem. Phys., 2017. **19**: p. 26210-26220.
11. Lu, J., et al., *Sinter-Resistant Catalysts: Supported Iridium Nanoclusters with Intrinsically Limited Sizes.* Catal. Lett., 2012. **142**: p. 1445-1451.
12. Bheemireddy, S.R., et al., *Contorted Aromatics via a Palladium-Catalyzed Cyclopentannulation Strategy.* J. Mater. Chem. C, 2016. **4**: p. 3963.
13. Yuan, B., et al., *Pentaleno[1,2-a:4,5']diacenaphthylenes: Uniquely Stabilized Pentalene*

Derivatives. J. Org. Chem., 2016. **81**: p. 8312.
14. Wang, L., C. Kalyanaraman, and A.B. McCoy, *Time-dependent quantum studies of the $O(^3P)$+ HCl reaction.* J. Chem. Phys., 1999. **110**: p. 11221-11232.
15. Yang, J., et al., *Effects of heterocyclic ring and amino-ethyl-amino group on the electronic and photophysical properties of a triphenylamine-pyrimidine dye.* Int. J. Quantum Chem., 2020. **120**: p. e26355.
16. Wang, T., et al., *Tuning electron–hole distance of the excitons in organic moleculesusing functional groups.* Chem. Phys. Lett., 2015. **618**: p. 142.
17. Zhou, X., et al., *Synthesis and photophysical studies of triazine-linked porphyrin-perylene bismide dyad with long-lived perylene triplet state.* J. Photochem. Photobiol. A: Chem., 2014. **274**: p. 57.
18. Wang, T., et al., *Effect of Triplet State on the Lifetime of Charge Separation in Ambipolar D-A_1-A_2 Organic Semiconductors.* J. Phys. Chem. C, 2016. **120**: p. 11338.
19. Wang, L. and G.D. Billing, *Rotational relaxation and transport properties of oxygen by using the important sampling method.* J. Phys. Chem. A, 1993. **97** p. 2523-2526.
20. Billing, G.D. and L. Wang, *Semiclassical calculations of transport coefficients and rotational relaxation of nitrogen at high temperatures.* J. Phys. Chem., 1992. **96**: p. 2572-2575.
21. Testoff, T.T., et al., *DFT studies of aggregation induced energy splitting and excitonic diversification in benzene and anthracene multimers.* Chem. Phys., 2022. **562**: p. 111641.
22. Xu, F., et al., *Cause, Regulation and Utilization of Dye Aggregation in Dye-Sensitized Solar Cells.* Molecules, 2020. **25**: p. 4478.
23. Weerasinghe, K.C., et al., *Coherently degenerate state engineering of organic small molecule materials to generate Wannier excitons.* Chem. Phys. Impact, 2022. **4**: p. 100062.
24. Wang, T., et al., *Ambipolar organic semiconductors with cascades of energy levels for generating long-lived charge separated states: a donor–acceptor1–acceptor2 architectural triarylamine dye.* J. Mater. Chem. C, 2014. **2**: p. 5466.
25. Wang, T., et al., *Enhancing Photoinduced Charge Separation through Donor Moiety in Donor-Accepter Organic Semiconductors".* J. Phys. Chem. C, 2016. **120**: p. 25263-25275.
26. Fan, X., et al., *Efficient photocatalytic dechlorination of chlorophenols over a nonlinear optical material $Na_3VO_2B_6O_{11}$ under UV-visible light irradiation.* J. Mater. Chem. A, 2015. **3**: p. 12179-12187.
27. Spivey, K., J.I. Williams, and L. Wang, *Structures of undecagold clusters: Ligand effect.* Chem. Phys. Lett., 2006. **432**: p. 163-166.
28. Fan, X., et al., *Exploring the Origin of High Dechlorination Activity in Polar Materials $M_2B_5O_9Cl$ (M= Ca, Sr, Ba, Pb) with Built-in Electric Field.* Chem. Mater., 2017. **29**: p. 639.
29. Sun, H., et al., *Enhanced Internal Quantum Efficiency in Dye-Sensitized Solar Cells: Effect of Long-Lived Charge-Separated State of Sensitizers.* ACS Appl. Mater. Interfaces, 2017. **9**: p. 9880.
30. Cheng, H.-W., et al., *A simple vaporous probe with atomic-scale sensitivity to structural ordering and orientation of molecular assembly.* Chem. Sci. , 2019. **10** p. 7104-7110.
31. Jaubert, J.-N.l., et al., *Benchmark Database Containing Binary-System-High-Quality-Certified Data for Cross-Comparing Thermodynamic Models and Assessing Their Accuracy.* Ind. Eng. Chem. Res., 2020. **59**: p. 14981−15027.
32. Lin, T., W. Zhang, and L. Wang, *Theoretical calculation of separation factors for boron*

isotopic exchange between BF_3 and $BF_3{\cdot}C_6H_5OCH_3$. J. Phys. Chem. A, 2009. **113** p. 7267-7274.

33. Salmani, H.J., et al., *Thermodynamic modeling of binary mixtures of ethylenediamine with water, methanol, ethanol, and 2-propanol by association theory.* RSC Adv., 2022. **12**: p. 32415.
34. Hao, Y. and C.-C. Chen, *Nonrandom two-liquid activity coefficient model with association theory.* AIChE J., 2021. **67**: p. e17061.
35. Ravichandran, A., R. Khare, and C.-C. Chen, *Predicting NRTL Binary Interaction Parameters from Molecular Simulations.* AIChE J., 2018. **64**: p. 2758-2769.
36. Kamath, G., G. Georgiev, and J.J. Potoff, *Molecular Modeling of Phase Behavior and Microstructure of Acetone-Chloroform-Methanol Binary Mixtures.* J. Phys. Chem. B, 2005. **109**: p. 19463-19473.
37. Keller, A., K. Langenbach, and H. Hasse, *Comparison of predictions of the PC-SAFT equation of state and molecular simulations for the metastable region of binary mixtures.* Fluid Phase Equilib., 2017. **444**: p. 31-36.
38. Vinhal, A.P.C.M., W. Yan, and G.M. Kontogeorgis, *Modeling the Critical and Phase Equilibrium Properties of Pure Fluids and Mixtures with the Crossover Cubic-Plus-Association Equation of State.* J. Chem. Eng. Data, 2020. **65**: p. 1095−1107.
39. Denis, S. and J.M. Prausnitz, *Statistical thermodynamics of liquid mixtures a new expression for the excess gibbs energy of partly or completely miscible systems.* AIChE J., 1975. **21**: p.116-128.
40. Luecke, R.H., *CORRELATIONS IN PUBLISHED VALUES OF UNIQUAC INTERACTION PARAMETERS.* Fluid Phase Equilibria, 1983. **14**: p. 373-382.
41. Kato, S., D. Hoshino, and H. Noritomi, *Prediction of activity coefficients using UNIQUAC interaction parameters correlated with constant-temperature VLE data for alkane alkane binaries.* Fluid Phase Equilibria, 2004. **219**: p. 41-47.
42. Jonsdottir, S.O., K. Rasmussen, and A. Fredenslund, *UNIQUAC parameters determined by molecular mechanics.* Fluid Phase Equilibria, 1994. **100**: p. 121-138.
43. Jonsdottir, S.O. and P. Rasjuussen, *Phase equilibria of carbohydrates in polar solvents.* Fliud Phase Equilibria, 1999. **158-160**: p. 411-418.
44. Jonsdottir, S.O., S.A. Cooke, and E.A. Macedo, *Modeling and measurements of solid–liquid and vapor–liquid equilibria of polyols and carbohydrates in aqueous solution.* Carbohydrate Research, 2002. **337**: p. 1563-1571.
45. Jonsdottir, S.O., K. Rasmussen, and P. Rasmussen, *Vapor liquid equilibria of polymer solutions determined by molecular mechanics.* Computational and Theoretical Polymer Science, 1998. **8**: p. 75-81.
46. Jonsdottir, S.O., R.A. Klein, and K. Rasmussen, *UNIQUAC interaction parameters for alkaneamine systems determined by Molecular Mechanics.* Fluid Phase Equilibria, 1996. **115**: p. 59-72.
47. Jonsdottir, S.O. and R.A. Klein, *UNIQUAC interaction parameters for molecules with -OH groups on adjacent carbon atoms in aqueous solution determined by molecular mechanics-glycols glycerol and glucose.* Fluid Phase Equilibria, 1997. **132**: p. 117-137.
48. Shi, J. and H. Li, *Modified temperature-dependent volume translation model in PC-SAFT equation of state for carbon dioxide.* Chem. Eng. Sci., 2022. **263**: p. 118107.

49. Plesu Popescu, A.E., et al., *Investigating best available technique for CO2 chemical absorption: solvent selection based on empirical surrogate model and energy loss.* Clean Technol. Environ. Policy, 2022. **24**(1): p. 333-350.
50. Nessi, E., et al., *Pilot scale assessment of a novel phase-change solvent for energy efficient post -combustion CO_2 capture.* J. Environ. Manage., 2022. **317**: p. 115489.
51. Olyaei, E., A. Hafizi, and M.R. Rahimpour, *Low energy phase change CO2 absorption using water-lean mixtures of glycine amino acid: Effect of co-solvent.* J. Mol. Liq., 2021. **336**: p. 116286.
52. Ochedi, F.O., et al., *Carbon dioxide capture using liquid absorption methods: a review.* Environ. Chem. Lett., 2021. **19**(1): p. 77-109.
53. Longeras, O., et al., *Tuning critical solution temperature for CO2 capture by aqueous solution of amine.* J. Mol. Liq., 2021. **343**: p. 117628.
54. Bobba, P., et al., *Solubility of Carbon Dioxide in Carboxylation Reaction Mixtures.* Ind. Eng. Chem. Res., 2021. **60**(23): p. 8375-8385.
55. Zheng, L., et al., *Simultaneous cooling and provision of make-up water by forward osmosis for post-combustion CO2 capture*. Desalination, 2020. **476**: p. 114215.
56. Zarogiannis, T., A.I. Papadopoulos, and P. Seferlis, *Efficient selection of conventional and phase-change CO2 capture solvents and mixtures based on process economic and operating criteria.* J. Cleaner Prod., 2020. **272**: p. 122764.
57. Papadopoulos, A.I., et al., *Phase-Change Solvents and Processes for Post-combustion CO2 Capture: A Detailed Review.* Ind. Eng. Chem. Res., 2019. **58**(13): p. 5088-5111.
58. Kazepidis, P., et al., *Optimal design of post combustion CO2 capture processes based on phase-change solvents.* Comput.-Aided Chem. Eng., 2019. **46**: p. 463-468.
59. Feng, H., et al., *Molecular Dynamics Simulation of Diffusion and Structure of Some n-Alkanes in near Critical and Supercritical Carbon Dioxide at Infinite Dilution.* J. Phys. Chem. B, 2013. **117**: p. 12525−12534.
60. KE, J., et al., *Detecting phase transitions in supercritical mixtures: an enabling tool for greener chemical reactions.* Proc. R. Soc. A, 2010. **466**: p. 2799-2818.
61. Santos, T.M.M., et al., *Dispersion Polymerization of Methyl Methacrylate in Supercritical CO2: A Preliminary Evaluation of In Situ Incorporation of Copaiba Oil.* Ind. Eng. Chem. Res., 2020. **59**(20): p. 9398-9407.
62. Rebelatto, E.A., et al., *Determination of high-pressure phase equilibrium data of systems containing supercritical carbon dioxide and globalide.* J. Supercrit. Fluids, 2020. **166**: p. 104996.
63. Fateen, S.-E.K., M.M. Khalil, and A.O. Elnabawy, *Semi-empirical correlation for binary interaction parameters of the Peng–Robinson equation of state with the van der Waals mixing rules for the prediction of high-pressure vapor–liquid equilibrium.* J. Adv. Res., 2013. **4**: p. 137-145.
64. Perdomo, F.A., et al., *A predictive group-contribution framework for the thermodynamic modelling of CO2 absorption in cyclic amines, alkyl polyamines, alkanolamines and phase-change amines: New data and SAFT-γ Mie parameters.* Fluid Phase Equilib., 2023. **566**: p. 113635.
65. Zid, S., et al., *Fluid phase equilibria for the CO2 + 2,3-dimethylbutane binary system from 291.9 K to 373.1 K.* J. Supercrit. Fluids, 2022. **179**: p. 105387.

66. Xiao, X., et al., *Isobaric heat capacity measurements on ternary mixtures of natural gas components methane, propane and n-heptane by differential scanning calorimetry at temperatures from 197 K to 422 K and pressures up to 32 MPa.* Fuel, 2022. **308**: p. 121904.
67. Tang, M., et al., *Experimental Measurements for Equilibrium Conditions of Carbon Dioxide Hydrate Mixtures with Each Additive of 1,3-Dioxane, Acetamide, Cyclopentanol, Cyclopentanone, or 1,3,5-Trioxane.* J. Chem. Eng. Data, 2022. **67**(10): p. 2954-2962.
68. Sanchez-Vicente, Y. and J.P.M. Trusler, *Saturated-Phase Densities of (CO2 + Methylcyclohexane) at Temperatures from 298 to 448 K and Pressures up to the Critical Pressure.* J. Chem. Eng. Data, 2022. **67**(1): p. 54-66.
69. Narayanan Nair, A.K., et al., *Bulk and Interfacial Properties of Brine or Alkane in the Presence of Carbon Dioxide, Methane, and Their Mixture.* Ind. Eng. Chem. Res., 2022. **61**(15): p. 5016-5029.
70. Li, M., et al., *Minimum miscibility pressure of CO2 and oil evaluated using MRI and NMR measurements.* J. Pet. Sci. Eng., 2022. **214**: p. 110515.
71. Kortsen, K., et al., *Exploiting the tuneable density of scCO2 to improve particle size control for dispersion polymerisations in the presence of poly(dimethyl siloxane) stabilisers.* Eur. Polym. J., 2022. **168**: p. 111108.
72. Kontos, G., et al., *Solubility of CO2 in 2-Amino-2-methyl-1-propanol (AMP) and 3-(Methylamino)propylamine (MAPA): Experimental Investigation and Modeling with the Cubic-Plus-Association and the Modified Kent-Eisenberg Models.* Separations, 2022. **9**(11): p. 338.
73. Kobayashi, K. and A. Firoozabadi, *Effect of Branching on Mutual Solubility of Alkane-CO_2 Systems by Molecular Simulations.* J. Phys. Chem. B, 2022. **126**(41): p. 8300-8308.
74. Aghel, B., et al., *Review on CO2 capture by blended amine solutions.* Int. J. Greenhouse Gas Control, 2022. **119**: p. 103715.
75. Papadopoulos, A.I., et al., *Molecular engineering of sustainable phase-change solvents: From digital design to scaling-up for CO2 capture.* Chem. Eng. J. (Amsterdam, Neth.), 2021. **420**(Part_2): p. 127624.
76. Sanchez-Vicente, Y., et al., *Density and Phase Behavior of the CO2 + Methylbenzene System in Wide Ranges of Temperatures and Pressures.* Ind. Eng. Chem. Res., 2020. **59**(15): p. 7224-7237.
77. Nascimento, J.C., et al., *Phase behavior of carbon dioxide + chloroform + ω-pentadecalactone + poly(ω-pentadecalactone) system: Experimental data and PC-SAFT modeling.* Fluid Phase Equilib., 2020. **521**: p. 112736.
78. Mayer, D.A., et al., *Effect of different polymer molar mass on the phase behavior of carbon dioxide + dichloromethane + ε-caprolactone + poly(ε-caprolactone) system.* Fluid Phase Equilib., 2020. **521**: p. 112687.
79. Wang, S., et al., *High-Pressure Vapor-Liquid Equilibria for a CO2 + p-Cymene Binary System at Temperatures from 313.15 to 353.15 K.* J. Chem. Eng. Data, 2019. **64**(12): p. 5584-5590.
80. Mayer, D.A., et al., *High Pressure Phase Equilibrium Data for the Ternary System Containing Carbon Dioxide, Dichloromethane, and ε-Caprolactone.* J. Chem. Eng. Data, 2019. **64**(5): p. 2036-2044.
81. Matsukawa, H., et al., *Phase behavior of a carbon dioxide/methyl trimethoxy*

silane/polystyrene ternary system. Polymers (Basel, Switz.), 2019. **11**(2): p. 246/1.
82. Leontiadis, K., et al., *Solubility of CO2 in 3-amino-1-propanol and in N-methyldiethanolamine aqueous solutions: Experimental investigation and correlation using the CPA equation of state.* Fluid Phase Equilib., 2019. **500**: p. 112254.
83. Al Ghafri, S.Z.S., et al., *Viscosity of (CH4 + C3H8 + CO2 + N2) mixtures at temperatures between (243 and 423) K and pressures between (1 and 28) MPa: Experiment and theory.* Fuel, 2019. **251**: p. 447-457.
84. Legoix, L.N., et al., *Phase Equilibria of the CH4-CO2 Binary and the CH_4-CO_2-H_2O Ternary Mixtures in the Presence of a CO_2-Rich Liquid Phase.* Energies, 2017. **10**: p. 2034.
85. De Guido, G. and E. Spatolisano, *Simultaneous Multiphase Flash and Stability Analysis Calculations Including Solid CO2 for CO2-CH4, CO2-CH4-N2, and CO2-CH4-N2-O2 Mixtures.* J. Chem. Eng. Data, 2021. **66**(11): p. 4132-4147.
86. Ababneh, H. and S.A. Al-Muhtaseb, *An empirical correlation-based model to predict solid-fluid phase equilibria and phase separation of the ternary system CH4-CO2-H2S.* J. Nat. Gas Sci. Eng., 2021. **94**: p. 104120.
87. Skarmoutsos, I., E. Guardia, and J. Samios, *Hydrogen bond, electron donor-acceptor dimer, and residence dynamics in supercritical CO_2-ethanol mixtures and the effect of hydrogen bonding on single reorientational and translational dynamics: A molecular dynamics simulation study.* J. Chem. Phys., 2010. **133**: p. 014504.
88. Mehl, A., et al., *Vapor-Liquid Equilibrium of Carbon Dioxide + Ethanol: ExperimentalMeasurements with AcousticMethod and ThermodynamicModeling.* J. Thermodyn., 2011: p. 251075,.
89. Jbari, Y. and S. Abderafi, *Liquid density prediction of ethanol/water, using artificial neural network.* Biointerface Res. Appl. Chem., 2022. **12**(4): p. 5625-5637.
90. Melfi, D.T., et al., *Kinetic Modeling of scCO2-Assisted Levulinic Acid Esterification with Ethanol Using Amberlyst-15 as a Catalyst in a Batch Reactor.* Energy Fuels, 2021. **35**(18): p. 14770-14779.
91. Liu, J., J. Qian, and H. Hu, *Effect of H2O on absorption performance of tetraethylenepentamine-ethanol-CO2 two-phase absorbent and its mechanism.* Int. J. Greenhouse Gas Control, 2021. **110**: p. 103406.
92. Jiang, Y., et al., *Impact mechanisms of supercritical CO2-ethanol-water on extraction behavior and chemical structure of eucalyptus lignin.* Int. J. Biol. Macromol., 2020. **161**: p. 1506-1515.
93. Chatzis, G. and J. Samios, *Binary mixtures of supercritical carbon dioxide with methanol. A molecular dynamics simulation study.* Chem. Phys. Lett., 2003. **374**: p. 187-193.
94. Yoon, J.-H., et al., *High-Pressure Phase Equilibria for Carbon Dioxide-Methanol-Water System: Experimental Data and Critical Evaluation of Mixing Rules.* Ind. Eng. Chem. Res., 1993. **32**: p. 2881-2887.
95. Mukhopadhyay, M., *Natural Extracts Using Supercritical Carbon Dioxide*. 2000: CRC Press.
96. Yu, C.-H., et al., *Modeling fluid phase equilibria of carbon dioxide-methanol binary system.* Fluid Phase Equilib., 2021. **529**: p. 112866.
97. F. London, Z., *Properties and applications of molecular forces.* Phys. Chem., 1930. **11**: p. 222-251.
98. Stone, A.J., *the theory of intermolecular forces*. 1996, Oxford: Clarendon Press.

99. Helgaker, T., P. Jorgensen, and J. Olsen, *Molecular Electronic-Structure Theory*. 2000, New York: J. Wiley.
100. Hobza, P., J. Sponer, and T. Reschel, *Density functional theory and molecular clusters.* J. Comput. Chem., 1995. **16**: p. 1315–1325.
101. Kristyan, S. and P. Pulay, *Can (semi)local density functional theory account for the London dispersion forces.* Chem. Phys. Lett., 1994. **229**: p. 175–180.
102. Lacks, D.J. and R.G. Gordon, *Pair interactions of rare gas atoms as a test of exchange-energy-density functionals in regions of large density gradients.* Phys. Rev. A, 1993. **47**: p. 4681-4690.
103. Jurečka, P. and P. J. Černý, *Density Functional Theory Augmented with an Empirical Dispersion Term. Interaction Energies and Geometries of 80 Noncovalent Complexes Compared with Ab Initio Quantum Mechanics Calculations.* J. Comput. Chem., 2007. **28**: p. 555-569.
104. Elstner, M., P. Hobza, and T. Frauenheim, *Hydrogen bonding and stacking interactions of nucleic acid base pairs: A density-functional-theory based treatment.* J. Chem. Phys., 2001. **114**: p. 5149-5155.
105. Grimme, S., *Semiempirical GGA-type density functional constructed with a long-range dispersion correction.* J. Comput. Chem., 2006. **27**: p. 1787-1799.
106. Grimme, S., *Accurate description of van der Waals complexes by density functional theory including empirical corrections.* J. Comput. Chem., 2004. **25**: p. 1463-1473.
107. Chai, J.D. and M.H. Gordon, *Long-range corrected hybrid density functionals with damped atom–atom dispersion corrections.* Phys. Chem. Chem. Phys., 2008. **10**: p. 6615-6620.
108. Grimme, S., J. Antony, and T. Schwabe, *Density functional theory with dispersion corrections for supramolecular structures, aggregates, and complexes of (bio)organic molecules* Org. Biomol. Chem., 2007. **5**: p. 741-758.
109. Hudson, G.A., et al., *Computational Studies on Response and Binding Selectivity of Fluoresence Sensors.* J. Phys. Chem. B, 2010. **114**: p. 870.
110. McCarroll, M.E., et al., *Computational prediction and experimental evaluation of a photoinduced electron-transfer sensor.* J. Phys. Chem. B, 2006. **110**: p. 22991.
111. Walkup, L.L., et al., *Importance of dynamics in electron excitation and transfer of organic dyes.* J. Phys. Chem. C, 2010. **114**: p. 19521.
112. Bondi, A., *Physical Properties of Crystals, Liquids and Glasses*. 1968, New York: John Wiley and Sons Inc.
113. S. Bock, E.B. and E. Vogel, *A new intermolecular potential energy surface for carbon dioxide from ab initio calculations.* Chem. Phys. , 2000. **257**: p. 147-156.
114. Steinebrunner, G., et al., *Structural and thermodynamic properties of fluid carbon dioxide from a new ab initio potential energy surface.* J. Chem. Phys., 1998. **109**(8): p. 3153-3160.
115. Tsuzuki, S., et al., *Intermolecular interaction potential of the carbon dioxide dimer* J. Chem. Phys., 1998. **109**: p. 2169-2175.
116. Décultot, M., et al., *Solubility of CO_2 in methanol, ethanol, 1,2-propanediol and glycerol from 283.15 K to 373.15 K and up to 6.0 MPa.* J. Chem. Thermodyn., 2019. **138**: p. 67-77.